Modeling the transfer of line edge roughness from an EUV mask to the wafer

Gregg M. Gallatin[a], Patrick P. Naulleau[b]
a Center for Nanoscale Science and Technology
National Institute of Standards and Technology, Gaithersburg, MD
b Center for X-Ray Optics, Lawrence Berkeley National Laboratory, Berkeley, CA

March 9, 2011

ABSTRACT

Contributions to line edge roughness (LER) from extreme ultraviolet (EUV) masks have recently been shown to be an issue of concern for both the accuracy of current resist evaluation tests as well the ultimate LER requirements for the 22 nm production node. More recently, it has been shown that the power spectral density of the mask-induced roughness is markedly different than that of intrinsic resist roughness and thus potentially serves as a mechanism for distinguishing mask effects from resist effects in experimental results. But the evaluation of stochastic effects in the resist itself demonstrate that such a test would only be viable in cases where the resist effects are completely negligible in terms of their contribution to the total LER compared to the mask effects. Also the results presented here lead us to the surprising conclusion that it is indeed possible for mask contributors to be the dominant source of LER while the spatial characteristics of the LER remain indistinguishable from the fractal characteristics of resist-induced LER.

1 Introduction

There are many contributors to line edge roughness (LER) in resist features on a wafer. The most widely studied contributor is the stochastic effect of exposure in the resist itself.[1,2,3,4] For EUV the contributions from the mask have recently been shown to be an issue of concern for both the accuracy of current resist evaluation tests as well the ultimate LER requirements for the 22 nm production node and beyond.[5] The power spectral density of the mask-induced roughness is markedly different from that of intrinsic stochastically generated resist roughness and thus could potentially serve as a mechanism for distinguishing mask effects from resist effects in experimental results. Here we study how the contributions coming from an EUV mask compare to the stochastic effects in the photoresist. Unfortunately, extraction of the mask contribution from wafer resist measurement is viable only in cases where the resist stochastic effects are almost completely negligible in terms of their contribution to the total LER. Surprisingly, even in that case, where the mask effects are dominant, it is possible for the spatial characteristics of the LER to remain indistinguishable from the fractal characteristics of stochastic resist-induced LER.

The paper is organized as follows. We start by discussing the two main mask contributors, mask LER and mask surface roughness. Section 2 describes the effect of LER on the mask and Section 3, the effect of roughness

of the reflective multilayer structure of the mask. The results in both sections are considered in terms of the aerial image. Section 4 shows wafer LER results for the combination of the two mask effects with the resist included but without stochastic effects in the resist. Section 5 briefly reviews resist stochastic effects from which we find that the spatial frequency content of the LER caused by the mask effects alone is very different from resist stochastic effects. In Section 6 we combine all the effects and find, somewhat surprisingly, that even when the mask contributions are by far dominant over the wafer stochastic contributions, the wafer LER frequency content is essentially indistinguishable in shape from that coming from the stochastic effects alone. Hence in a practical sense one cannot separate out the individual contributions from the mask and wafer just by examining the wafer resist LER.

2 Mask LER effect on aerial images

The effect that the optics have on the transfer of mask to wafer LER can be quantified using the LER Transfer Function or LTF.[6] The form of this function can be derived analytically in terms of the effect that mask LER has on the image at the wafer. Assume that the nominal line edge corresponds to the x axis thus the image intensity depends only on y and has the value $I(y=0)=I_{\mathrm{th}}$. The mask LER causes a fluctuation in the intensity and moves the positions where the image intensity equals I_{th} away from $y=0$. Assuming the resist development process always places the edge so as to satisfy $I(y)=I_{th}$ then a fluctuation in the intensity, $I(y)\rightarrow I(y)+\delta I(x,y)$ will be compensated by a change in the edge position on the wafer given by $\delta y_{\mathrm{wafer}}(x)$. Since the nominal position is $y=0$ we have

$$I\left(\delta y_{\mathrm{wafer}}(x)\right)+\delta I\left(x,\delta y_{\mathrm{wafer}}(x)\right)=I_{\mathrm{th}} \tag{1}$$

The dependence of $\delta y_{\mathrm{wafer}}$ on x follows implicitly from demanding that $\delta y_{\mathrm{wafer}}$ satisfy the above equation at each position x along the edge. Expanding to first order in $\delta y_{\mathrm{wafer}}(x)$ we find that $\delta y_{\mathrm{wafer}}$ and δI must be the same order of smallness and so we can drop the $\delta I\delta y_{\mathrm{wafer}}$ cross term leaving

$$I(0)+S(x)\,\delta y_{\mathrm{wafer}}(x)+\delta I(x,0)=I_{\mathrm{th}} \tag{2}$$

where $S=\left.\frac{dI(y)}{dy}\right|_{y=0}$ is the image slope in the y direction which for the case at hand is independent of x Using $I(0)=I_{\mathrm{th}}$ and rearranging gives

$$\delta y_{\mathrm{wafer}}(x)=\frac{\delta I(x,0)}{S}=\frac{\delta I(x,0)}{I_{\mathrm{th}}\times ILS} \tag{3}$$

after using $S/I(0)=S/I_{\mathrm{th}}=$ the image log slope or ILS.

Now consider the edge on the mask that defines the edge on wafer. Let the mask edge deviation that generates $\delta y_{\mathrm{wafer}}(x)$ be $\delta y_{\mathrm{mask}}(x)$. Using the standard Hopkins equation[6] to compute $\delta I(x,0)$ we find to lowest order in δy_{mask}

$$\delta\tilde{y}_{\mathrm{wafer}}(\beta)=LTF(\beta)\,\delta\tilde{y}_{\mathrm{mask}}(\beta) \tag{4}$$

where $\delta\tilde{y}_{wafer}(\beta)$ and $\delta\tilde{y}_{mask}(\beta)$ are the Fourier transforms respectively of $\delta y_{wafer}(x)$ and $\delta y_{mask}(x)$, in wafer plane coordinates and $\beta=2\pi f$ with f the spatial frequency of the roughness. For tophat pupil fill $\sigma$and numerical aperture NA we find[6]

$$LTF(\beta)=\frac{\int ds\,\mathrm{Re}\left(\sqrt{\sigma^2-s^2}\right)\mathrm{Re}\left(\sqrt{1-(s-\beta/NAk)^2}\right)}{\int ds\,\mathrm{Re}\left(\sqrt{\sigma^2-s^2}\right)\mathrm{Re}\left(\sqrt{1-s^2}\right)} \tag{5}$$

where $k=2\pi/\lambda$ with λ being the wavelength of the light. The denominator is included so that $LTF(0)=1$. Analytical results are shown in Figure 1. Comparison to full numerical simulation can be found in.[6]

Finally note that the effect of mask LER is not restricted to EUV systems alone but also appears in deep ultraviolet (DUV) and other imaging systems.

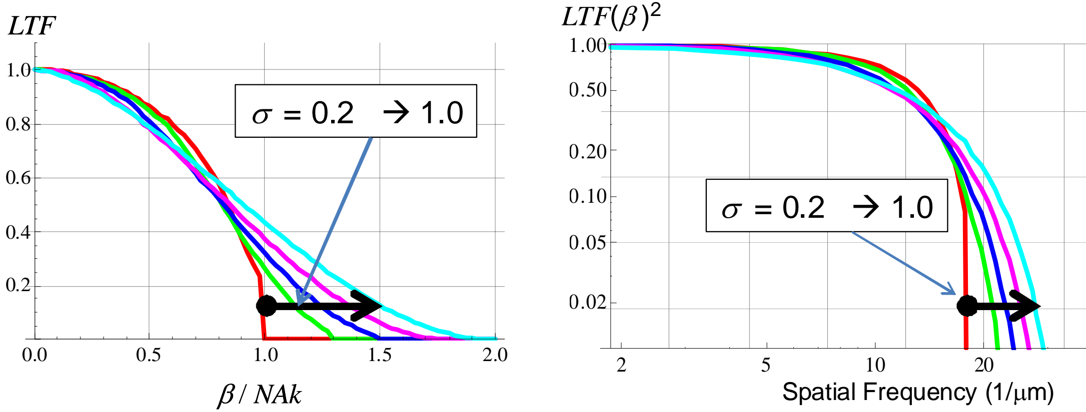

Figure 1: The left graph shows the $LTF\left(\beta\right)$ plotted for tophat fill factors $\sigma=0.2,\ 0.4,\ 0.6,\ 0.8,\ 1.0$. The function has a distinct shoulder shape for the smaller values of σ.The LTF is plotted on a linear scale in the graph on the left and LTF^2 is plotted on a log-log scale in the graph on the right. This makes it easy to compare the LTF to the power spectral densities (PSDs) of the roughness which are the square of the spatial frequency content of the LER and are commonly plotted on a log-log scale. The values $NA=0.25$ and $\lambda=13.5$ nm were used in the right hand graph to convert β/NAk to spatial frequency.

3 EUV mask surface roughness effect on aerial images

EUV masks consist of a patterned absorber layer on top of a reflective multilayer stack. Previous work has shown that phase variations in the multilayer have the same effect optically as reflection from a rough surface, i.e., the reflected wavefront carries an imprint of the surface but with twice the amplitude.[5,7,8] It is also possible to include reflectivity variations in the same way but we will not do so here.

There are two effects caused by EUV mask surface roughness. Unfortunately unlike the mask LER, these effects don't yield a simple analytical transfer function like the LTF and the results shown in Figure 2 are derived from image simulations which account for partial coherence and the specific aberrations of the Berkeley microfield exposure tool (MET) as well as surface roughness.[5]

In order to understand the origin of the two effects consider a single, and hence perfectly coherent, plane wave incident normally on a surface with the deviation from perfect planarity being given by $h\left(x,y\right)$. Then up to an an overall constant factor the reflected field ϕ will have the form $\exp\left[-2ikh\left(x,y\right)\right]\equiv\exp\left[2\pi iw\left(x,y\right)\right]$ where $w\left(x,y\right)$ is the wavefront in waves. Since ϕ is pure phase the reflected intensity $I=\left|\phi\right|^2=1$ and so is perfectly uniform as desired. But it's the field at the wafer that counts and there are two relevant effects that occur in projecting the field onto the wafer plane. First, the projection optics filters out spatial frequencies that do not lie inside the NA of the optics. Second, the field at the wafer cannot be in perfect focus everywhere. There are always slight variations in the axial position of best focus across the field of view, the wafer itself is not perfectly flat and finally even in the absence of these inherent errors, noise, thermal fluctuations and bandwidth limitations of the focusing system itself make it impossible to hold the system in perfect focus everywhere and at all times. These two effects are combined in the point spread function P of the optics which depends both on the NA and the amount of defocus. Using P, the field at the wafer can be written as

$$\phi_{\mathrm{wafer}}\left(x,y,z\right)=\int dx'dy'P\left(x-x',y-y',z\right)\exp\left[2\pi iw\left(x',y'\right)\right] \tag{6}$$

where z is the amount of defocus and we are representing everything in wafer scale coordinates. If the spatial frequency content of $\exp\left[2\pi iw\left(x,y\right)\right]$ lies completely within the NA of the optics then and the system is in focus,

$z = 0$, only then will we have

$$\begin{aligned}\phi_{\text{wafer}}(x,y,0) &= \int dx'dy' P(x-x', y-y', 0) \exp[2\pi i w(x',y')] \\ &= \exp[2\pi i w(x,y)] \end{aligned} \tag{7}$$

and so $I_{\text{wafer}}(x,y) \equiv |\phi_{\text{wafer}}(x,y)|^2 = 1$ and the intensity at the wafer plane would be uniform. But even if the frequency content of $w(x,y)$ itself lies completely inside the NA the higher order terms in $\exp[2\pi i w(x,y)] = 1 + 2\pi i w(x,y) - 2\pi^2 w(x,y)^2 + \cdots$ will contain higher and higher spatial frequencies which do not fit inside the NA and so in general for almost any $w(x,y)$ we have

$$\begin{aligned}I_{\text{wafer}}(x,y,0) &= \left| \int dx'dy' P(x-x', y-y', 0) \exp[2\pi i w(x',y')] \right|^2 \\ &\neq |\exp[2\pi i w(x,y)]|^2 \end{aligned} \tag{8}$$

Thus in general $I_{\text{wafer}}(x,y) \equiv |\phi_{\text{wafer}}(x,y)|^2 \neq 1$ even in focus. The intensity is not uniform but speckled, with the statistical properties of the speckle following from the statistical properties of the mask roughness $w(x,y) = -(k/\pi) h(x,y)$.

The effect of defocus, either positive or negative, will be to increase the speckle. The reason for this is simple. In areas where the downstream pointing normals to the wavefront surface $w(x,y) =$ constant are converging, the field will become more focussed and hence more intense if the focus is shifted downstream. Conversely in areas where the downstream normals are diverging the field will be defocussed and hence become less intense if the focal position is shifted in the downstream direction. The opposite happens if the focus position is shifted in the upstream direction. Hence the effect of defocus either, positive or negative, is to increase the amplitude of the speckle. Both these effects are clearly visible in the results shown in Figure 2 which are derived from thresholding the aerial image exactly as in the previous section. A simple "rule-of-thumb" can be used to estimate the effect of the surface roughness.[9]

4 Mask LER and surface roughness effects in resist

Resist is added to the model by including the following equations.[10,11,12]

$$\rho_{\text{acid}}(\vec{r},0) = \rho_{\text{PAG}}(1 - \exp[-\alpha q I(\vec{r}) t_{\exp}]) \tag{9}$$

$$\frac{\partial \rho_{\text{D}}(\vec{r},t)}{\partial t} = -k\rho_{\text{acid}}(\vec{r},t)(1-\rho_{\text{D}}(\vec{r},t)) \tag{10}$$

$$\frac{\partial \rho_{\text{acid}}(\vec{r},t)}{\partial t} = D_{\text{acid}} \vec{\nabla}^2 \rho_{\text{acid}}(\vec{r},t) - g\rho_{\text{acid}}(\vec{r},t)\rho_{\text{base}}(\vec{r},t) \tag{11}$$

$$\frac{\partial \rho_{\text{base}}(\vec{r},t)}{\partial t} = D_{\text{base}} \vec{\nabla}^2 \rho_{\text{base}}(\vec{r},t) - g\rho_{\text{acid}}(\vec{r},t)\rho_{\text{base}}(\vec{r},t) \tag{12}$$

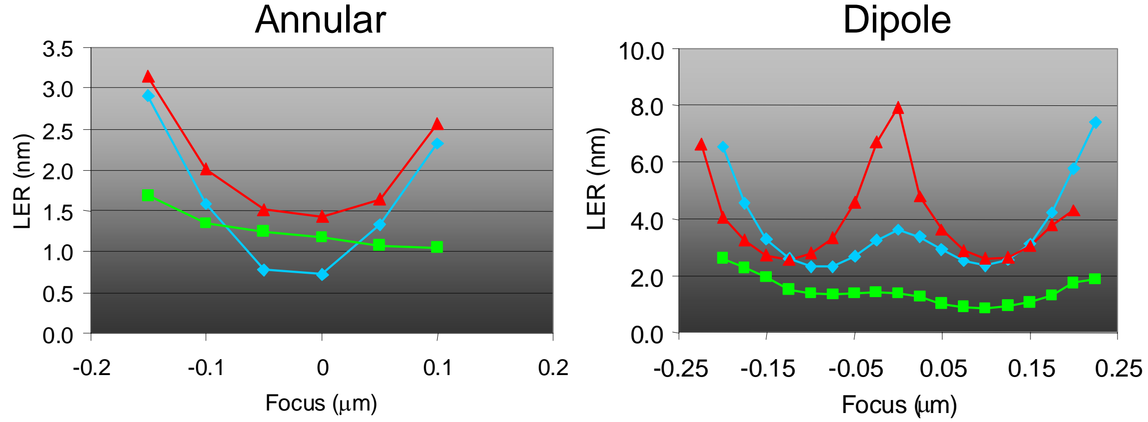

Figure 2: The graphs show simulated LER for annular and dipole illumination for a 50 nm line/space patterin. The flare and aberrations used in the image calculations correspond to the Berkeley MET.[18] The annular illumination σ was 0.35 to 0.55 and the dipole illumination had $\sigma = 0.2$ poles centered at ± 0.36 in the pupil. The diamond data is the contribution from multilayer roughness alone, the square data is the contribution from mask LER alone and the triangle data is the combination of both. It follows from this result that, at least for the particular statistics used in this case for the roughness and mask LER that the roughness is the dominant contributor. The root mean square variation in the LER based on the statistics of the mask LER and surface roughness is approximately 0.1 nm.

where

$$
\begin{aligned}
\rho_{\text{acid}}(\vec{r},t) &= \text{\# of acid molecules/volume at } \vec{r} \text{ at time } t \\
\rho_{\text{base}}(\vec{r},t) &= \text{\# of base molecules/volume at } \vec{r} \text{ at time } t \\
\rho_{\text{D}}(\vec{r},t) &= \text{Density of deprotection in the resist at } \vec{r} \text{ at time } t \\
\rho_{\text{PAG}} &= \text{\# of photo acid generator (PAG) molecules/volume loaded into the resist} \\
\alpha &= \text{Resist absorptivity (\# of photons absorbed/length)} \\
q &= \text{Photon-PAG interaction volume} \\
k &= \text{Deprotection rate constant (units = area/time in 2D and volume/time in 3D)} \\
I(\vec{r}) &= \text{Intensity at position } \vec{r} \text{ during exposure (\# of photons/(area} \times \text{time)} \\
t_{\text{exp}} &= \text{Total exposure time} \\
D_{\text{acid}} &= \text{Acid diffusion contsant (units = length/time}^{1/2}\text{)} \\
D_{\text{base}} &= \text{Base diffusion constant (units = length/time}^{1/2}\text{)} \\
g &= \text{Acid base neutralization rate constant (units = volume/time)}
\end{aligned}
$$

The aerial image intensity $I(\vec{r})$ is calculated as before. Eq (9) accounts for exposure of the resist. Given a resist absorptivity α, photon-PAG interaction volume q and post exposure bake (PEB) time t_{PEB} the initial acid distribution $\rho_{\text{acid}}(\vec{r},0)$ is computed from Eq (9). Eqs (10-12) account for the deprotection of the resist during PEB. We assume that the initial base loading $\rho_{\text{base}}(\vec{r},t)$ is uniform throughout the resist and that $\rho_{\text{D}}(\vec{r},0) = 0$. The technique we use for solving the equations is the following. Eqs (10-12) are analytically solvable in 1D, 2D and 3D when $g = 0$ and Eqs (11-12) are analytically solvable when $D_{\text{acid}} = D_{\text{base}} = 0$. The $g = 0$ solutions of

Eqs (11-12) take the form of an appropriate point spread function P acting on the given density, e.g.,

$$\begin{aligned}
\rho_{\text{acid}}\left(\vec{r},t+\Delta t\right) &= \int d^n r' P_{\text{acid}}\left(\vec{r}-\vec{r}',\Delta t\right)\rho_{\text{acid}}\left(\vec{r},t\right) \\
&= \left(4\pi D_{\text{acid}}\Delta t\right)^{-n/2}\int d^n r' \exp\left[-\left(\vec{r}-\vec{r}'\right)/4D_{\text{acid}}\Delta t\right]\rho_{\text{acid}}\left(\vec{r},t\right) \\
\rho_{\text{base}}\left(\vec{r},t+\Delta t\right) &= \int d^n r' P_{\text{base}}\left(\vec{r}-\vec{r}',\Delta t\right)\rho_{\text{base}}\left(\vec{r},t\right) \\
&= \left(4\pi D_{\text{base}}\Delta t\right)^{-n/2}\int d^n r' \exp\left[-\left(\vec{r}-\vec{r}'\right)/4D_{\text{base}}\Delta t\right]\rho_{\text{base}}\left(\vec{r},t\right) \qquad (13)
\end{aligned}$$

where n is the number of space dimensions. The solution for the deprotection is

$$\rho_{\text{D}}\left(\vec{r},t+\Delta t\right) = 1-\exp\left[-k\int_t^{t+\Delta t} dt' \rho_{\text{acid}}\left(\vec{r},t'\right)\right] \qquad (14)$$

The solution for Eqs (11-12) with $D_{\text{acid}} = D_{\text{base}} = 0$ is

$$\begin{aligned}
\rho_{\text{acid}}\left(\vec{r},t+\Delta t\right) &= \frac{\rho_{\text{acid}}\left(\vec{r},t\right)\left(\rho_{acid}\left(\vec{r},t\right)-\rho_{\text{base}}\left(\vec{r},t\right)\right)\exp\left[g\left(\rho_{\text{acid}}\left(\vec{r},t\right)-\rho_{\text{base}}\left(\vec{r},t\right)\right)\left(t+\Delta t\right)\right]}{\rho_{\text{base}}\left(\vec{r},t\right)-\rho_{\text{acid}}\left(\vec{r},t\right)\exp\left[g\left(\rho_{\text{acid}}\left(\vec{r},t\right)-\rho_{\text{base}}\left(\vec{r},t\right)\right)\left(t+\Delta t\right)\right]} \\
\rho_{\text{base}}\left(\vec{r},t+\Delta t\right) &= \rho_{\text{acid}}\left(\vec{r},t+\Delta t\right)-\left(\rho_{\text{acid}}\left(\vec{r},t\right)-\rho_{\text{base}}\left(\vec{r},t\right)\right) \qquad (15)
\end{aligned}$$

The solutions given in Eqs (13-15) are valid for any two times t and $t+\Delta t$ with $\Delta t > 0$. Hence we could have used 0 and some total time T instead of t and $t+\Delta t$.The reason for using t and $t+\Delta t$ is that the solution approach used here is to iterate between the solutions given in Eqs (13-14) and in Eq (15)[10] That is, turn off the diffusion (set $D_{\text{acid}} = D_{\text{base}} = 0$) and solve for ρ_{acid} and ρ_{base} at time $t+\Delta t$ given their values everwhere at time t using Eq (15). Then turn off acid base neutralization (set $g = 0$) and use the solutions in Eqs (13-14) to solve for $\rho_{\text{acid}}, \rho_{\text{base}}$ and ρ_{D} at time $t+2\Delta t$ using the values obtained from the first step at time $t+\Delta t$. Note that during the acid base neutralization time step the deprotection density is assumed to not change. Starting at $t = 0$ this process is iterated N times until the total time $N\Delta t = t_{\text{PEB}}$.

Although the solutions in Eq (13) are valid in 3D ($n = 3$) we will simplify things here by assuming that the exposure intensity is uniform through the resist thickness, i.e., in z, and integrate out the z dependence in the point spread functions. This effectively reduces the problem to 2D ($n = 2$). Further we will assume that $g\Delta t$ is large enough to drive the acid base neutralization to completion during it's Δt time step. In the limit as $g\Delta t \rightarrow \infty$ the solutions in Eq (15) become

$$\begin{aligned}
\rho_{\text{acid}}\left(\vec{r},t+\Delta t\right) &= \begin{cases} \rho_{\text{acid}}\left(\vec{r},t\right)-\rho_{\text{base}}\left(\vec{r},t\right) \text{ where } \rho_{\text{acid}}\left(\vec{r},t\right)-\rho_{\text{base}}\left(\vec{r},t\right) > 0 \\ 0 \text{ where } \rho_{\text{acid}}\left(\vec{r},t\right)-\rho_{\text{base}}\left(\vec{r},t\right) < 0 \end{cases} \\
\rho_{\text{base}}\left(\vec{r},t+\Delta t\right) &= \begin{cases} 0 \text{ where } \rho_{\text{base}}\left(\vec{r},t\right)-\rho_{\text{acid}}\left(\vec{r},t\right) < 0 \\ \rho_{\text{base}}\left(\vec{r},t\right)-\rho_{\text{acid}}\left(\vec{r},t\right) \text{ where } \rho_{\text{base}}\left(\vec{r},t\right)-\rho_{\text{acid}}\left(\vec{r},t\right) > 0 \end{cases} \qquad (16)
\end{aligned}$$

Here we use a 4 step iteration to represent the entire PEB and assume the base does not diffuse, $D_{\text{base}} = 0$ in any time step. Interestingly the algorithm can actually run faster if shorter time steps are used even though this requires more iterations. This is because for shorter times the size of the matrices needed to represent the point spread functions P_{acid} and P_{base} can be smaller while maintaining the same spatial resolution since during shorter times there is less diffusion. In the limit as $\Delta t \rightarrow 0$ this approach devolves to the standard finite difference time domain (FDTD) approach.

The final step, resist development is treated as a threshold on the deprotection density. That is at positions $\vec{r}$ where $\rho_D\left(\vec{r},t_{\text{PEB}}\right) > \rho_{\text{th}}$ the resist is assumed be completely dissolved away and at positions $\vec{r}$ where $\rho_D\left(\vec{r},t_{\text{PEB}}\right) < \rho_{\text{th}}$ to remain.

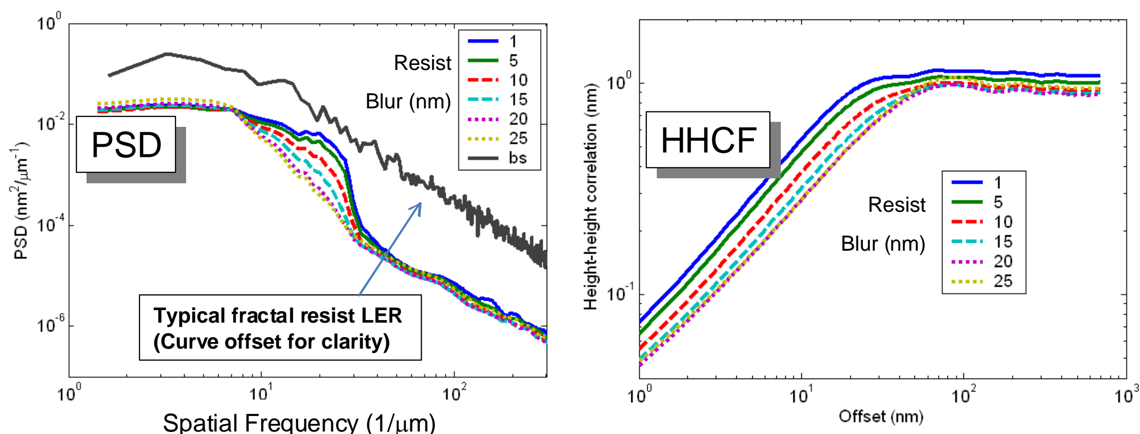

Figure 3: LER PSD and HHCF computed from the resist deprotection density. No resist stochastics are included. The mask LER and roughness statistics, Berkely MET flare, aberrations and dipole illumination are the same as those used in Figure 3. The effect of the LTF is clearly evident as the bump at spatial frequencies of around $20/\mu m$ and at the smaller resist blur values. There is very little evidence of mask effects in the HHCF. A typical resist PSD is shown for comparison. It has been offset from the other curves for clarity.

Using the measured statistics for mask LER and roughness we generated 10 representative masks and computed resist line edges for those masks and from that the mean power spectral density (PSD) and height-height correlation function (HHCF) of the resist LER for various values of the resist blur, which in this case is simply $R = \sqrt{D_{\text{acid}} t_{\text{PEB}}}$ since we have taken $D_{\text{base}} = 0$, and for various values of the deprotection rate constant k. The results are shown in Figure 3. The existence of a distinct bump in the PSD caused by the LTF raises the possibility of fitting wafer LER PSD data to determine directly the mask LER and roughness contribution. Unfortunately when resist stochastics are included as described in the next section this possibility practically disappears.

5 Mask LER and surface roughness effects combined with resist stochastics

There are several sources of stochastic behavior in the exposure and development of photoresist. The primary one is wave function collapse.[13] When a photon is absorbed by the resist all of its energy goes into one molecule or atom of the resist. Hence, the smooth continuous aerial image is captured by the resist as the distribution of points (atoms or molecules) where the photons are absorbed. This is illustrated in Figure 4 and is generally referred to as photon shot noise. There are also stochastic effects in the chemistry of the PEB and the development step but for DUV resists these effects are much smaller than that caused by wave function collapse.[1] At EUV wavelengths on the other hand there is a second source of stochastic effects which may not be negligable. This source follows from the mechanism of exposure of an EUV resist. At DUV wavelengths, in a chemically amplified resist the acids which do the deprotection are released predominantly only when the photon is absorbed by a PAG molecule. The photons that are absorbed by other molecules are similar to those that pass through the resist in that they cause no relevant chemical changes in the resist. Their absorption does decrease the remaining numbers of photons which does affect the final acid distribution but only indirectly. EUV photons have an energy of about 92 eV, as opposed to DUV photons which have energies on the around 5 eV. Hence the aborption of an EUV photon by any molecule or atom in the resist generally produces a photoelectron. This photoelectron can have an energy close to the EUV photon energy and as it travels through the resist can generate secondary

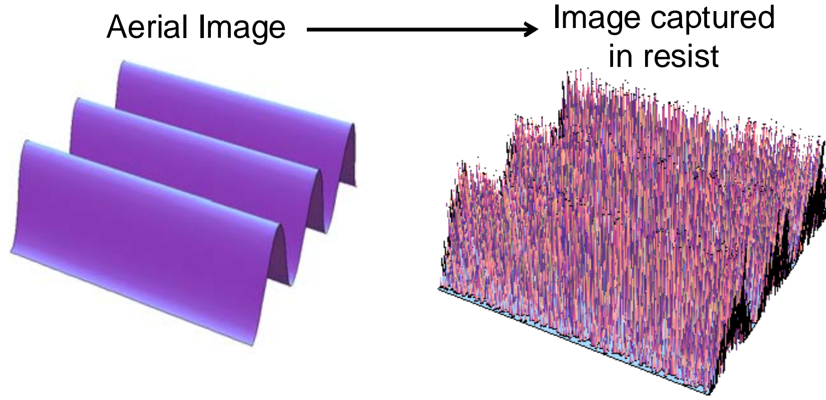

Figure 4: The effect of exposure statistics is shown here. On the left is the aerial image plotted as usual as a continuous surface. On the right is the result of exposing that aerial image in the resist. For the computation of the Poisson statistics as discussed in the text, the pixel size was taken to be 1 nm^2 and the exposure dose corresponds to 5 mJ/cm^2.

electrons and when any of these electrons, primary or secondary, interacts with a PAG molecule they can cause it to release an acid. The process of secondary electron generation is certainly stochastic[2,3,4] and is often referred to as acid shot noise. It also adds to net effective blur of the resist.[14,15] To get absolute values for LER both these effects should be included with the proper scaling but in many cases the LER is dominated by the photon shot noise and so to illustrate the effect of stochastics on the results of the previous sections we will consider just photon shot noise.

To include photon shot noise in the model we apply a Poisson distribution to the number of photons actually absorbed in a given pixel rather than using the nominal number. That is, if the nominal number of photons absorbed in a given pixel is N, in the model that number is replaced by the a number chosen randomly from the Poisson distribution defined by

$$p\left(n|N\right) = \frac{N^n}{n!}e^{-N}$$

Here $p\left(n|N\right)$ indicates the probability of getting n when the average value is N.

The effect of the stochastics varies with dose and to study this we vary the base loading to adjust the dose to size. The results for the PSD are shown in Figure 5. The bump that was present in the PSD in the nonstochastic case has effectively dissapeared. For the 32 mJ/cm^2 case the total LER was 2.6 ± 0.1 nm while the mask only contribution to the LER was 2.2 ± 0.1 nm. The mask and resist processes are statistically independent and so we can estimate that the direct resist stochastic contribution to the LER is $\sqrt{(2.6 \pm 0.1 \text{ nm})^2 - (2.2 \pm 0.1 \text{ nm})^2} \approx$ 1.4 ± 0.4 nm. The 32 mJ/cm^2 PSD shows little or no evidence of a mask induced bump and so we see that even when the mask induced LER on the order of twice the resist stochastic induced LER the effect of the mask is basically invisible in the resist PSD.

A comparison of the values of the critical exponent α computed from the PSD and from the HHCF are shown in Figure 6 along with the LWR and LER results for the case shown in Figure 5. The critical exponent α characterizes how the HHCF scales at small shifts, i.e., HHCF $\propto$ (shift/correlation length)$^\alpha$ for shifts much less than the correlation length. The critical exponent is related to the negative of the slope of the PSD on a log-log scale, γ, by $\alpha = 2\gamma + 1$.[16] The analytically predicted form of the LER[1] has $\gamma = 3$ which corresponds to $\alpha = 1$.The

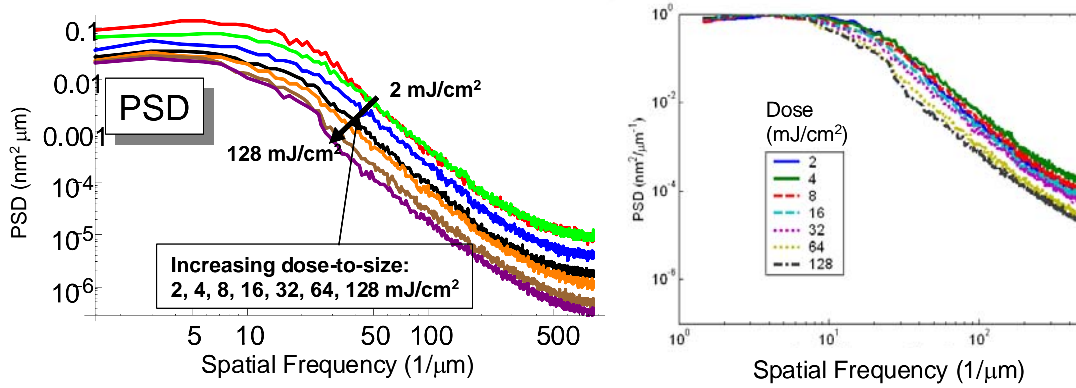

Figure 5: The resist PSD including stochastic effects in the resist such as those shown in Figure 4. The imaging conditions match those in Figure 3. The value of k was 4 nm^3/s and the resist blur was set to 10 nm. With the inclusion of resist stochastic effects the bump in the PSD has virtually disappeared although some remnant of it appears visible at the highest doses.

results shown in Figure 6 are in line with that prediction. The fact that α is close to unity indicates that the PSD has the self-affine character of the typical resist PSD as shown in Figure 3

6 Conclusion

We have shown how mask LER and surface roughness are mapped to wafer LER in various scenarios. In the absence of stochastic effects in the resist the mask LER and roughness are visible as a bump in the wafer resist PSD but the bump disappears when resist stochastic effects are included. Hence, for practical purposes, the mask contribution to the resist LER cannot be determined simply by examining the resist PSD. The mask contribution must be measured in a more direct fashion.such as described in[17]

E_{size} (mJ/cm^2)	α PSD	α HHCF	LWR (nm)	LER (nm)
2	0.94	0.75	9.8 ± 0.1	6.7 ± 0.1
4	0.91	0.7	7.6 ± 0.1	5.3 ± 0.1
8	0.94	0.71	5.7 ± 0.1	4.1 ± 0.1
16	0.93	0.74	4.4 ± 0.1	3.2 ± 0.1
32	0.94	0.74	3.9 ± 0.1	2.8 ± 0.1
64	0.92	0.76	3.3 ± 0.1	2.4 ± 0.1
128	0.8	0.78	3.0 ± 0.1	2.3 ± 0.1

Figure 6: Values of the critical exponent α computed from the PSD and the HHCF along with the corresponding LER and LWR values for the cases shown in Figure 5.

7 REFERENCES

[1] G. M. Gallatin, Proc. SPIE **5754**, 38 (2005).

[2] D. Drygiannakis, et. al., Proc. SPIE **6519**, 65193T (2007).

[3] J. Biafore, et. al., Proc. SPIE **7636**, 76360R-1 (2010).

[4] C. Mack, et. al., Proc SPIE **7969**, 7969-43, to appear, (2011).

[5] P. P. Naulleau, J. Vac. Sci. Technol. **B 26**, 1289 (2008).

[6] P. P. Naulleau and G. M. Gallatin, Appl. Opt. **42**, 3390 (20003).

[7] P. P. Naulleau and G. M. Gallatin, J. Vac. Sci. Technol. **B 26**, 1903 (2008).

[8] S. A. George, et. al., Proc SPIE **7969**, 7969-13, to appear (2010).

[9] B. M. McClinton and P. P. Naulleau, Proc SPIE **7636**, 76362G-2 (2010).

[10] H. Fukuda, et. al., Proc. SPIE **4346**, 319 (2001).

[11] P. P. Naulleau, G. M. Gallatin, J. Vac. Sci. Technol. **B 28**, 1259 (2010).

[12] C. Mack, *Fundamental Principles of Optical Lithography* (Wiley, West Sussex, England, 2007, Chapter 7, page 257).

[13] R. P. Feynman, R. Leighton and M. Sands, *The Feynman Lectures on Physics* (Addison-Wesley 1965, Vol 3. Chapter 1).

[14] C. N. Anderson, et. al., J. Vac. Sci. Technol. **B 26**, 2295 (2008).

[15] G. M. Gallatin, et. al., Proc. SPIE **6519**, 651911 (2007).

[16] V. Constantoudis, et. al., Proc SPIE **5038**, 901 (2003).

[17] P. P. Naulleau, et. al., Proc. SPIE **7636**, 76361J (2010).

[18] J. Cain, et. al., J. Vac. Sci. Technol. **B 24**, 1234 (2006).